PTRANSP Simulation and Experimental Test of a Robust Current Profile and β_N Controller for Off-axis Current Drive Scenarios in the DIII-D Tokamak

Wenyu Shi, William Wehner, Justin Barton, Mark D. Boyer, Eugenio Schuster, Arnold Kritz, Didier Moreau, Tim C. Luce, John R. Ferron, Michael L. Walker, David A. Humphreys, Ben G. Penaflor and Robert Johnson

***Abstract*— During the tokamak discharge, especially the ramp-up phase, the plasma state equilibrium continually evolves. As a consequence, the plasma response model should evolve as well. We first identified a linear plasma response model of the rotational transform ι profile and β_N around a desired equilibrium. Then, an uncertainty is introduced to the identified model to partially account for the dynamic character of the plasma state equilibrium evolution. A robust controller is designed to stabilize this family of plasma models, which are reformulated into a nominal model with uncertainty. A singular value decomposition (SVD) of the nominal identified model is carried out to decouple and identify the most relevant control channels in steady-state. The *DK*-iteration method, combining H_∞ synthesis and μ analysis, is applied to synthesize a closed-loop controller that minimizes the tracking error and input effort. The feedback controller is then augmented with an anti-windup compensator, which keeps the given profile controller well-behaved in the presence of magnitude constraints in the actuators and leaves the nominal closed-loop unmodified when no saturation is present. PTRANSP simulations and experimental results in DIII-D illustrate the performance of the model-based controller.**

I. Introduction

The goal of advanced tokamak (AT) research in the DIII-D tokamak is to develop the scientific basis for steady state, high-performance operation in ITER. Setting up a desirable current profile in the device is essential to certain AT operating scenarios. The plasma rotational transform ι profile is related to the current profile in the tokamak, and the shape of the ι profile is related to the development of a self generated, non-inductive source of current in the plasma. Another key performance parameter, β_N, defined as a ratio between the internal kinetic pressure of the plasma and the external pressure of the magnetic field, represents a measure of efficiency of confinement in the tokamak. This paper aims at designing a robust ι profile and β_N controller for high-confinement mode (H-mode) discharges in DIII-D.

As an alternative to the first-principles-driven methods, system identification techniques [1] have the potential to develop low-complexity, linear, dynamic models around a particular equilibrium. A two-time-scale linear current profile model with on-axis neutral beam injection has been identified for JET [2], and a toroidal rotation profile model has been estimated for JT-60U [3], [4]. System identification experiments with on-axis current drive (CD) have also been carried out on the DIII-D tokamak [4], and we have previously proposed identified models of the rotational transform profile [5], the toroidal rotation profile [6] and the rotational transform profile combined with β_N [7].

In this work, we extend our previous work [5], [7] in many important areas. Firstly, the off-axis current drive is introduced to the experiments, which could provide more heating in the mid-radius of the tokamak that would not be possible with only on-axis current drive. Secondly, the start time of the control phase is moved backward from the current flat-top phase to the current ramp-up phase. In order to increase the validity range of the identified model, we increase/decrease the singular values of the identified model to form a series of models to cover a neighborhood of the desired equilibrium. *DK*-iteration, combining H_∞ synthesis and μ analysis, is applied to synthesize a closed-loop controller that minimizes the control error and optimizes input effort. Then, the robust controller is successfully tested in the PTRANSP code [8], a tokamak transport analysis code, before experiments to evaluate the influence of the off-axis current drive system in DIII-D. Finally, a profile control experiment integrating magnetic and kinetic variables on DIII-D illustrates the performance of the proposed controller.

This paper is organized as follows. In Section II, the system identification process used for the DIII-D tokamak is briefly described, and a linear dynamic model of the ι profile and β_N is developed. In Section III, the designs of the plasma control algorithm and the anti-windup compensator are described. Closed-loop PTRANSP simulated results with off-axis CD are presented in Section IV, and experimental results from the DIII-D tokamak are presented in Section V. Section VI states the conclusions.

II. System Identification on DIII-D

The ι profile is defined as the inverse of the safety factor q profile, where q is the ratio of the number of times a magnetic field line goes toroidally around the tokamak to the number of times it goes around poloidally. High q_{min} scenario development at high β_N has been limited in our previous work [7] due to the overdrive of the central current by the on-axis NBI. Off-axis NBI can provide a broad current deposition at mid-radius without over-driving the current near the axis [9]. To achieve higher β_N and higher

This work was supported by the National Science Foundation CAREER Award program (ECCS-0645086), and the U.S. Department of Energy (DE-FG02-09ER55064 and DE-FC02-04ER54698). W. Shi (wenyu.shi@lehigh.edu), W. Wehner, J. Barton, M.D. Boyer and E. Schuster are with the Department of Mechanical Engineering & Mechanics, Lehigh University, Bethlehem, PA 18015, USA. A. Kritz is with the Department of Physics, Lehigh University, Bethlehem, PA 18015, USA. D. Moreau is with CEA, IRFM, 13108 Saint-Paul-lez-Durance, France. T.C. Luce, J.R. Ferron, M.L. Walker, D.A. Humphreys, B.G. Penaflor, and R. Johnson are with General Atomics, San Diego, CA 92121, USA.

q_{min}, the beam-line optical axes of 150L and 150R were inclined up to 16.5°, while the other beam-line optical axes were unchanged. The available beam-lines and gyrotrons were grouped to form, together with I_p, five independent H&CD actuators: (*i*) plasma current I_p, (*ii*) on-axis co-current NBI power P_{CO} (330L), (*iii*) off-axis co-current NBI power P_{OA} (150L and 150R), (*iv*) counter-current NBI power P_{CT} (210R), and (*v*) total EC power from all gyrotrons P_{EC}.

Several shots (#140076, 140077, 140093, 140106, and 140107)) [6] were used to identify the plasma response to the on-axis actuators. To collect the data for identifying the response of the off-axis beams (150L and 150R), a new shot #150082 with off-axis beams was run, while the other actuators were modulated around the identical reference values as the previous shots. System identification for the plasma rotational transform profile $\iota(\hat{\rho})$ was carried out with 5 Galerkin coefficients computed at normalized radial coordinates $\hat{\rho} = 0.2, 0.4, 0.5, 0.6, 0.8$, starting at $t = 2.5s$. The parameter $\hat{\rho}$ is the normalized effective minor radius, which is denoted as $\hat{\rho} = \frac{\rho}{\rho_b}$, where ρ is the mean effective minor radius of the flux surface, i.e., $\pi B_{\phi,0}\rho^2 = \Phi$. The parameter Φ is the toroidal magnetic flux, and $B_{\phi,0}$ is the magnetic field at the geometric major radius. The parameter ρ_b is the effective minor radius of the last closed magnetic flux surface.

The relation between inputs and outputs for any discharge is assumed in the form of

$$y(t) = y_{FF} + \Delta y(t) = P_{FF}(u_{FF}) + P\Delta u(t), \qquad (1)$$

where P_{FF} represents the relationship between the reference (feedforward) input u_{FF} and the reference (feedforward) output y_{FF}. The variable $\Delta y(t)$ denotes the deviation output defined as $\Delta y(t) = [\Delta\iota(t),\ \Delta\beta_N(t)] = y(t) - y_{FF}$, with $y(t) = [\iota(0.2,t)\ \iota(0.4,t)\ \iota(0.5,t)\ \iota(0.6,t)\ \iota(0.8,t),\ \beta_N(t)]^T$. The variable $\Delta u(t)$ denotes the deviation input defined as $\Delta u = u - u_{FF}$ with $u = [I_p,\ P_{CO},\ P_{OA},\ P_{CT},\ P_{EC}]$. By subtracting the feedforward value from our data set, we only consider the linear dynamics $\Delta y(t) = P\Delta u(t)$. The linear model P is identified from experimental data using the prediction error method (PEM) according to a least squares fit criterion [1]. The identified feedback model P can be expressed in the state space form

$$\dot{x} = Ax(t) + B\Delta u(t), \qquad \Delta y(t) = Cx(t) \qquad (2)$$

where the state $x(t)$ is defined as $x(t) = \Delta\iota(t) = \iota(t) - \iota_{FF}$. More details of the system identification process can be obtained from our previous work [5], [6], [7].

III. Control System Design

A. Singular Value Decomposition

The relation between the inputs and the outputs in the linear dynamic model (2) can be expressed in terms of its transfer function $P(s)$, i.e., $\frac{\Delta Y(s)}{\Delta U(s)} = P(s) = C(sI - A)^{-1}B$, where s denotes the Laplace variable and $\Delta Y(s)$ and $\Delta U(s)$ denote the Laplace transforms of the output Δy and the input Δu respectively. Assuming a constant target $\Delta\bar{y}_{tar}$ and closed-loop stabilization, the system will reach steady state as $t \to \infty$. It is possible to define $\Delta\bar{y} = \lim_{t\to\infty}\Delta y(t)$, $\Delta\bar{u} = \lim_{t\to\infty}\Delta u(t)$,

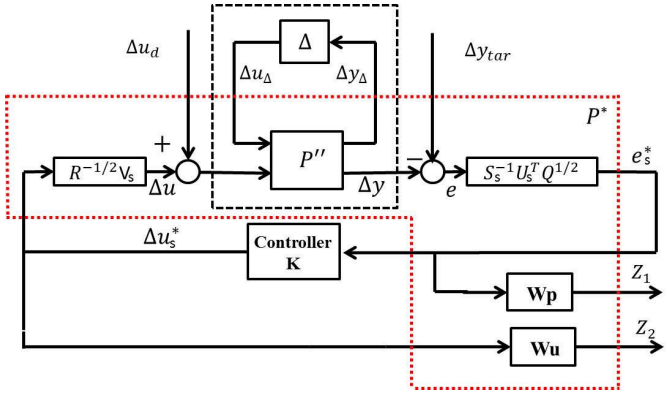

Fig. 1. Mixed-sensitivity H_∞ control problem.

and $\bar{e} = \lim_{t\to\infty} e(t) = \Delta\bar{y}_{tar} - \Delta\bar{y}$. Therefore, under these assumptions the closed-loop system is specified by

$$\Delta\bar{y} = \bar{P}\Delta\bar{u} = -CA^{-1}B\Delta\bar{u} \quad \Delta\bar{u} = \hat{\bar{K}}\bar{e}, \qquad (3)$$

where $\hat{K}(s)$ represents the transfer function of the to-be-designed controller and $\hat{\bar{K}} = \hat{K}(0)$.

In order to weight the control effort and tracking error, two positive definite weighting matrices $R \in \Re^{m\times m}$ and $Q \in \Re^{p\times p}$ are introduced to the system, where $p = 6$ is the number of outputs and $m = 5$ is the number of inputs. We then define the "weighted" steady-state transfer function, and its singular value decomposition (SVD) as $\bar{P} = Q^{1/2}\bar{P}R^{-1/2} = USV^T$, where $S = \mathrm{diag}(\sigma_1, \sigma_2, \cdots, \sigma_m) \in \Re^{m\times m}$, $U \in \Re^{p\times m}$ ($U^TU = I$), and $V \in \Re^{m\times m}$ ($V^TV = VV^T = I$). By invoking the properties of the SVD, the matrix $Q^{-1/2}US$ defines a basis of the steady-state output values, and the matrix $R^{-1/2}V$ defines a basis of the steady-state input values. By defining $\Delta\bar{y}^* = S^{-1}U^TQ^{1/2}\Delta\bar{y}$, $\Delta\bar{y}^*_{tar} = S^{-1}U^TQ^{1/2}\Delta\bar{y}_{tar}$, and $\Delta\bar{u}^* = V^TR^{1/2}\Delta\bar{u}$, a square decoupled system is obtained:

$$\Delta\bar{y}^* = S^{-1}U^TQ^{1/2}\Delta\bar{y} = S^{-1}U^TQ^{1/2}Q^{-1/2}USV^TR^{1/2}\Delta\bar{u} = \Delta\bar{u}^*.$$

Substituting these expressions into the performance index $\bar{J} = \bar{e}Q\bar{e}^T$, we can obtain the steady state cost function:

$$\bar{J} = (\Delta\bar{y}^*_{tar} - \Delta\bar{y}^*)^TS^2(\Delta\bar{y}^*_{tar} - \Delta\bar{y}^*) = \sum_{i=1}^{m}\sigma_i^2(\Delta\bar{y}^*_{tar_i} - \Delta\bar{y}^*_i)^2.$$

It is usually the case where $\sigma_1 > \cdots \sigma_k \gg \sigma_{k+1} > \cdots > \sigma_m > 0$. To avoid spending a lot of control effort for a marginal improvement of the cost function value, we partition the singular value set into significant singular values S_s and negligible singular values S_n. We can write $U = \begin{bmatrix} U_s & U_n \end{bmatrix}$, $V = \begin{bmatrix} V_s & V_n \end{bmatrix}$, $S = \mathrm{diag}(S_s,\ S_n)$, and approximate the cost function $\bar{J}$ by

$$\bar{J}_s = \sum_{i=1}^{k}\sigma_i^2(\Delta\bar{y}^*_{tar_i} - \Delta\bar{y}^*_i)^2 = (\Delta\bar{y}^*_{tar_s} - \Delta\bar{y}^*_s)^TS_s^2(\Delta\bar{y}^*_{tar_s} - \Delta\bar{y}^*_s),$$

where $\Delta\bar{y}^*_{tar_s} = S_s^{-1}U_s^TQ^{1/2}\Delta\bar{y}_{tar}$, $\Delta\bar{y}^*_s = S_s^{-1}U_s^TQ^{1/2}\Delta\bar{y}$, $\bar{e}^*_s = \Delta\bar{y}^*_{tar_s} - \Delta\bar{y}^*_s$ and $\Delta\bar{u}^*_s = V_s^TR^{1/2}\Delta\bar{u}$. The matrix bases reduce to $Q^{-1/2}U_sS_s$ and $R^{-1/2}V_s$, and the decoupled system,

$$P_{DC} = S_s^{-1}U_s^TQ^{1/2}PR^{-1/2}V_s, \qquad (4)$$

represents a one-to-one relationship between the inputs $\Delta\bar{u}^*_s$ and the outputs $\Delta\bar{y}^*_s$. More details of SVD can be obtained from our previous work [5], [7].

B. Design of μ Synthesis Controller

The plasma state continually changes during the plasma current ramp-up phase, and as a result, the plasma response model (2) should change. In order to partially account for this, we define the decoupled identified model P_{DC} (4) as the nominal model, and assume the singular values of the system P_{DC} can increase/decrease to form a broad frequency range covering a neighborhood of plasma states, which define a range of uncertainty ΔP. The new plasma model can be considered as the sum of P_{DC} with uncertainty ΔP, which is formulated into a robust control framework. There is always a trade-off between the performance of the controller and the robustness properties of the closed-loop system. The maximum increasing/decreasing magnitude of the singular values represents the desired robustness level of the closed-loop system. In this work, the singular values S_s are assumed to increase and decrease 20% to attempt to capture the dynamic character of the plasma state equilibrium evolution during the current ramp-up phase.

The decoupled system P_{DC} (4) based on P (2) is chosen as the nominal model, which is denoted as P_0. The singular values S_s decrease 20% to obtain a new system $P_{DC_t} = (0.8S_s^{-1})U_s^T Q^{1/2} P R^{-1/2} V_s$, which is denoted as P_{top}, and has the highest magnitude over the frequency range considered. The singular values S_s increase 20% to obtain another new system $P_{DC_b} = (1.2S_s^{-1})U_s^T Q^{1/2} P R^{-1/2} V_s$, which is denoted as P_{bot}, and has the lowest magnitude. The top and bottom uncertainty can be expressed in state-space form as:

$$\Delta A_i = A_i - A_0 \qquad \Delta B_i = B_i - B_0$$
$$\Delta C_i = C_i - C_0 \qquad \Delta D_i = D_i - D_0$$

where the subscript $i \in 1,2$ refers to the top and bottom respectively. The state-space system matrices are now written as uncertain matrices as

$$A = A_0 + \sum_{i=1}^{2} \delta_i \Delta A_i \quad B = B_0 + \sum_{i=1}^{2} \delta_i \Delta B_i$$
$$C = C_0 + \sum_{i=1}^{2} \delta_i \Delta C_i \quad D = D_0 + \sum_{i=1}^{2} \delta_i \Delta D_i \tag{5}$$

where $\delta_1 \in [0,1]$ and $\delta_2 \in [0,1]$.

By exploiting the structure of the state matrices (5) and using SVD, the system can be expressed in the conventional $P'' - \Delta$ control framework (black dashed block in Fig. 1), by employing the method outlined in [10]. See [11] for an example of this technique. Using the partition of the generalized plant $P'' = \begin{bmatrix} P''_{11} & P''_{12} \\ P''_{21} & P''_{22} \end{bmatrix}$, the input/output equations are

$$\Delta y_\Delta = P''_{11}\Delta u_\Delta + P''_{12}(\Delta u^*_s + \Delta u^*_{d_s}),$$
$$\Delta y = P''_{21}\Delta u_\Delta + P''_{22}(\Delta u^*_s + \Delta u^*_{d_s}),$$

where $\Delta u^*_s = V_s^T R^{1/2} \Delta u$, $\Delta u^*_{d_s} = V_s^T R^{1/2} \Delta u_d$, and Δu_d is the input disturbance.

The control goal is to design a $k \times k$ feedback controller K, where k is the number of significant singular values. The corresponding block diagram of the system is shown in Fig. 1 where the weight functions $W_p(s)$ and $W_u(s)$ are parameterized as

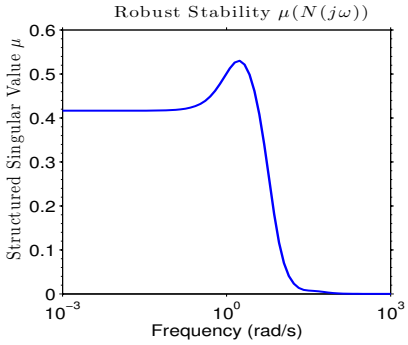

Fig. 2. Structured Singular Value μ versus Frequency

$$W_p(s) = K_p \left(\frac{\frac{s}{M_1} + w_{b1}}{s + w_{b1} A_1} \right)^2, \; W_u(s) = K_u \left(\frac{s + w_{b2} A_2}{\frac{s}{M_2} + w_{b2}} \right)^2$$

and the coefficients M_i, A_i, w_{bi}, for $i \in 1,2$, as well as K_p and K_u, are design parameters.

The feedback system can now be expressed in the conventional $\Delta - P^* - K$ robust control framework, where Δ is the uncertainty, P^* is the generalized plant (red dotted block in Fig. 1) , K is the feedback controller, and $[Z_1^T, Z_2^T]^T = [(W_p e^*_s)^T, (W_u \Delta u^*_s)^T]^T$ is the weighted performance signal. The closed-loop transfer function from the input $[\Delta y^{*T}_{tar_s}, \Delta u^{*T}_{d_s}]^T$ to the output $\begin{bmatrix} Z_1^T & Z_2^T \end{bmatrix}^T$ is defined as

$$T_{zr} = F_u(N, \Delta), \tag{6}$$

where $\Delta y^*_{tar_s} = S_s^{-1} U_s^T Q^{1/2} \Delta y_{tar}$, $\Delta y^*_s = S_s^{-1} U_s^T Q^{1/2} \Delta y$, $e^*_s = \Delta y^*_{tar_s} - \Delta y^*_s$, and the subsystem

$$N = F_l(P^*, K) = \begin{bmatrix} W_p M_s & -W_p M_s P''_{22} \\ W_u K M_s & -W_u K M_s \end{bmatrix}. \tag{7}$$

The sensitivity transfer function M_s is defined as $M_s = (I + P''_{22} K)^{-1}$. We seek a controller $K(s)$ that robustly stabilizes the system and minimizes the H_∞ norm of the transfer function $T_{zr}(N, \Delta)$, i.e.,

$$\min_{K(s)} \|T_{zr}(N,\Delta)\|_\infty = \min_{K(s)} (\sup_\omega \bar{\sigma}[T_{zr}(N,\Delta)(j\omega)]), \tag{8}$$

where $\bar{\sigma}$ represents the maximum singular value. The control method employed in this work to achieve the control goal (8) is the μ synthesis design technique.

There is no direct method to synthesize a μ-optimal controller, however the DK-iteration method [10], which combines H_∞ synthesis and μ analysis, can be used to obtain an iterative solution. This method starts with an upper bound on μ in terms of the scaled singular value $\mu(N) \leq \min(\bar{\sigma}(DND^{-1}))$. Then, we seek a controller that minimizes the peak value over frequency of this upper bound

$$\min_K (\min \left\| DN(K)D^{-1} \right\|_\infty).$$

To validate the designed controller, the robust stability of the closed-loop system is determined. The system is written in the $N - \Delta$ structure, and the robust stability is determined by evaluating the structured singular value

$$\mu(N_{11}(j\omega)) = \frac{1}{\min\{k_m | \det(I - k_m N_{11} \Delta) = 0\}} \tag{9}$$

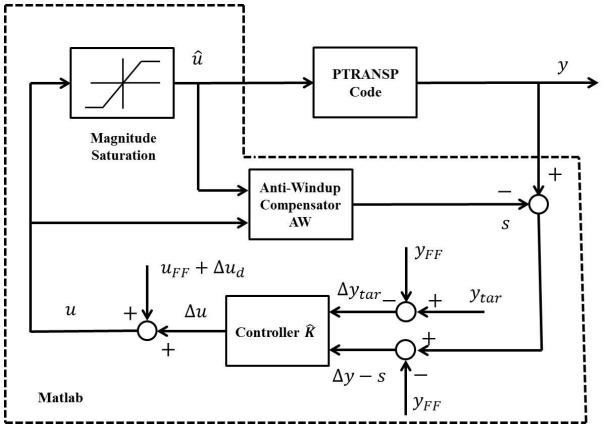

Fig. 3. The architecture of the closed-loop PTRANSP simulation.

where N_{11} is the transfer function from the input Δu_Δ to the output Δy_Δ. The closed-loop system is robustly stable for all allowable perturbations if and only if $\mu(N_{11}(j\omega)) < 1, \forall \omega$. Fig. 2 shows a plot of the structed singular value μ versus frequency, and as can be seen $\mu < 1$ for all frequencies. Therefore, the closed-loop system is robustly stable. In other words, the controller stabilizes the whole family of models.

In practice, the control input and measured output of the original system P are Δu and Δy, respectively. The measured output is in turn used to compute the tracking error $e = \Delta y_{tar} - \Delta y$. As shown in Fig. 1, the overall ι-profile and β_N controller for system P can be computed as

$$\hat{K}(s) = \frac{\Delta U(s)}{E(s)} = R^{-1/2} V_s K(s) S_s^{-1} U_s^T Q^{1/2} \qquad (10)$$

where $\Delta U(s)$ and $E(s)$ denotes the Laplace transforms of Δu and e, respectively.

C. Design of the Anti-windup Compensator

At the moment of designing the robust MIMO controller (10), the actuator saturations were not considered. As a result of saturation, the actual plant input may be different from the output of the controller. The goal is not to redesign the proposed MIMO controller but to design an anti-windup compensator that keeps the controller well-behaved and avoid undesirable oscillations when saturation is present. The anti-windup compensator must in addition leave the nominal closed-loop unmodified when no saturation is present. Details of the anti-windup compensation can be obtained from our previous work [5], [7].

IV. Closed-loop PTRANSP Simulations

In PTRANSP, experimental data is used directly to calculate the plasma state evolution without feedback. In order to form the closed-loop simulation, we combined the PTRANSP code with Matlab. A general framework for closed-loop feedback control implemented in PTRANSP is shown in Fig. 3. The PTRANSP solver is set to evolve in time only the ι profile based on the updated I_p, beam powers (P_{CO}, P_{OA}, and P_{CT}), and EC power P_{EC} output by the feedback controller. The feedback portion of the controller was implemented as a discrete time state-space controller with a sampling time of 20 milliseconds, because the controller implemented in DIII-D PCS has a sampling time of 20 milliseconds. The PTRANSP calculation stops every 20 milliseconds, and sends the calculated output y to Matlab. Based on the tracking error, Matlab calculates the next step input $\hat{u}$, and sends it back to PTRANSP. Then the PTRANSP code calculates the plasma state evolution for the next 20 milliseconds. This configuration provides us the ability to test the feedback controller in reference tracking and disturbance rejection simulations before experiments.

The reference shot for PTRANSP is shot #147626, which is a shot with off-axis neutral beam injection, and the feedforward inputs and target ι profiles are shown in Fig. 4 (red dashed line). The feedback controller is turned on at $t = 2.5$ s, and the disturbance is introduced at $t = 3$ s, which are $\delta I_p = 0.1$ MA, $\delta P_{CO} = -0.1$ MW, $\delta P_{OA} = 0$ MW, $\delta P_{CT} = 0$ MW, and $\delta P_{EC} = -0.3$ MW. An important goal of the model-based current profile controller is to regulate ι profile in the center precisely, since this affects confinement and stability for advanced scenarios. In order to reach this goal, we take $Q = \mathrm{diag}([5,\ 2.5,\ 1.5,\ 1.5,\ 1.5,\ 0.5])$ to weight the tracking errors, and the control weight matrix is redefined as $R = \mathrm{diag}([0.5,\ 0.1,\ 0.1,\ 0.1,\ 0.05])$. The parameter c for the anti-windup compensator is set as 0.1.

The simulated closed-loop-controlled inputs (solid blue lines) are shown in Fig. 4 (a) and compared with the reference open-loop inputs (red dashed lines) and another feedforward open-loop inputs with disturbance (dot-dash line). The simulated closed-loop-controlled ι profile at $\hat{\rho} = 0.2, 0.4, 0.5, 0.6, 0.8$ (solid blue lines) are shown in Fig. 4 (b) and compared with the target values (red dashed lines) and the feedforward open-loop outputs with disturbance (dot-dash line). By examining Fig. 4 (b) , we see that with feedforward control only the target profile is not achieved in the presence of the disturbance. In the first 0.5 second of the closed-loop simulation, from $t = 2.5$ s to $t = 3$ s, the controller works well, and the ι profile is regulated around the target values. Then the disturbance is introduced into the system at $t = 3$ s, and the plasma current, beam and gyrotron powers are modulated around their reference values without saturation by the feedback controller. Due to the design of the weight matrix Q, the control effort is mainly applied to $\iota(0.2,t)$ and $\iota(0.4,t)$, and the controller increases P_{OA} and the total EC power P_{EC} and requests the I_p to decrease to drive the system towards the desired inner ι profile. Note that the inner ι profile response is much slower than the boundary ι profile response, and the effect of the control effort on the inner ι profile is shown with a time delay. This is due to the high temperature and slow diffusivity in the core relative to the boundary. Improved performance can be observed from the comparison between the controlled results (solid blue line) and uncontrolled results (dotted-dashed line).

V. Experimental Results on DIII-D

In order to compare relevant experimental results with PTRANSP simulation, the same controller was applied and the same input disturbances were introduced in the experiment. The target ι profile and β_N obtained from shot #147634

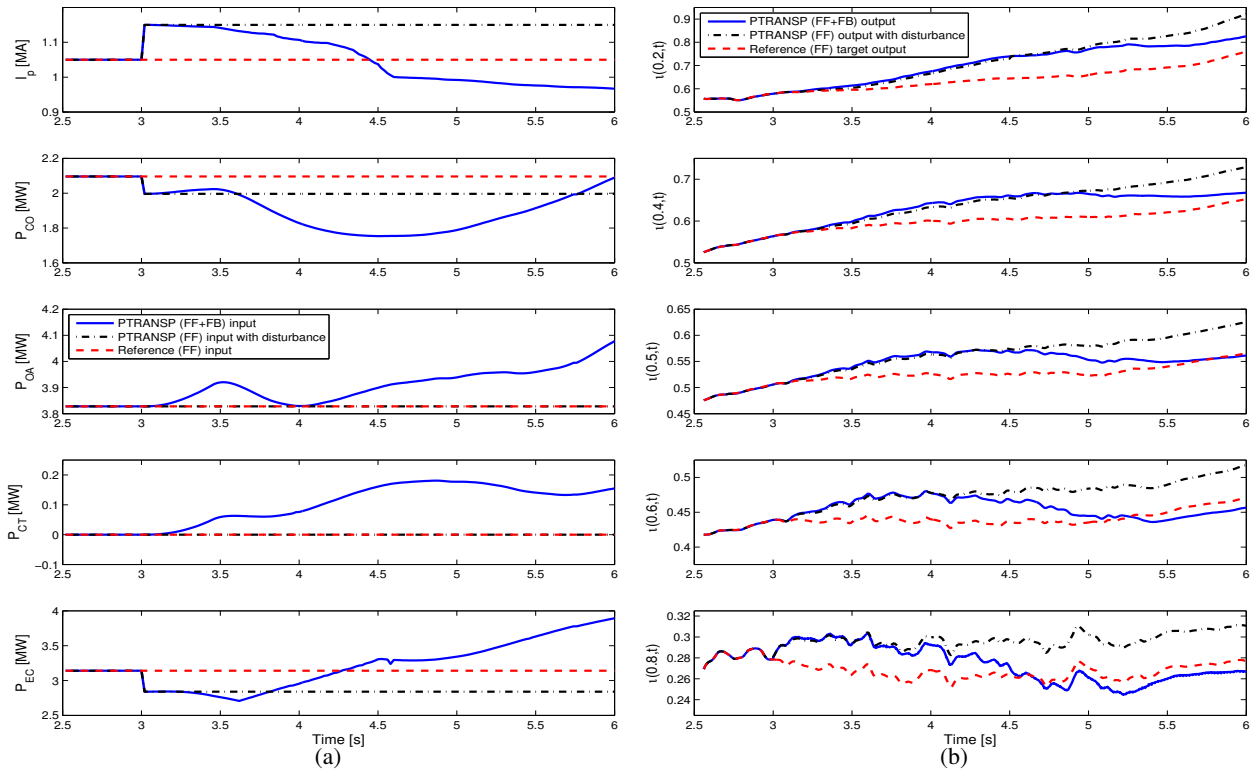

Fig. 4. PTRANSP simulation of rotational transform ι profile control with off-axis NBI: (a) Reference (feedforward) inputs (red dashed lines), feedforward inputs with disturbance (black dotted-dashed line) and feedforward+feedback control inputs (blue solid lines); (b) Reference target ι profile (red dashed lines), feedforward with disturbance ι profile (black dotted-dashed line) and feedforward+feedback ι profile at $\hat{\rho} = 0.2, 0.4, 0.5, 0.6, 0.8$ (solid blue lines).

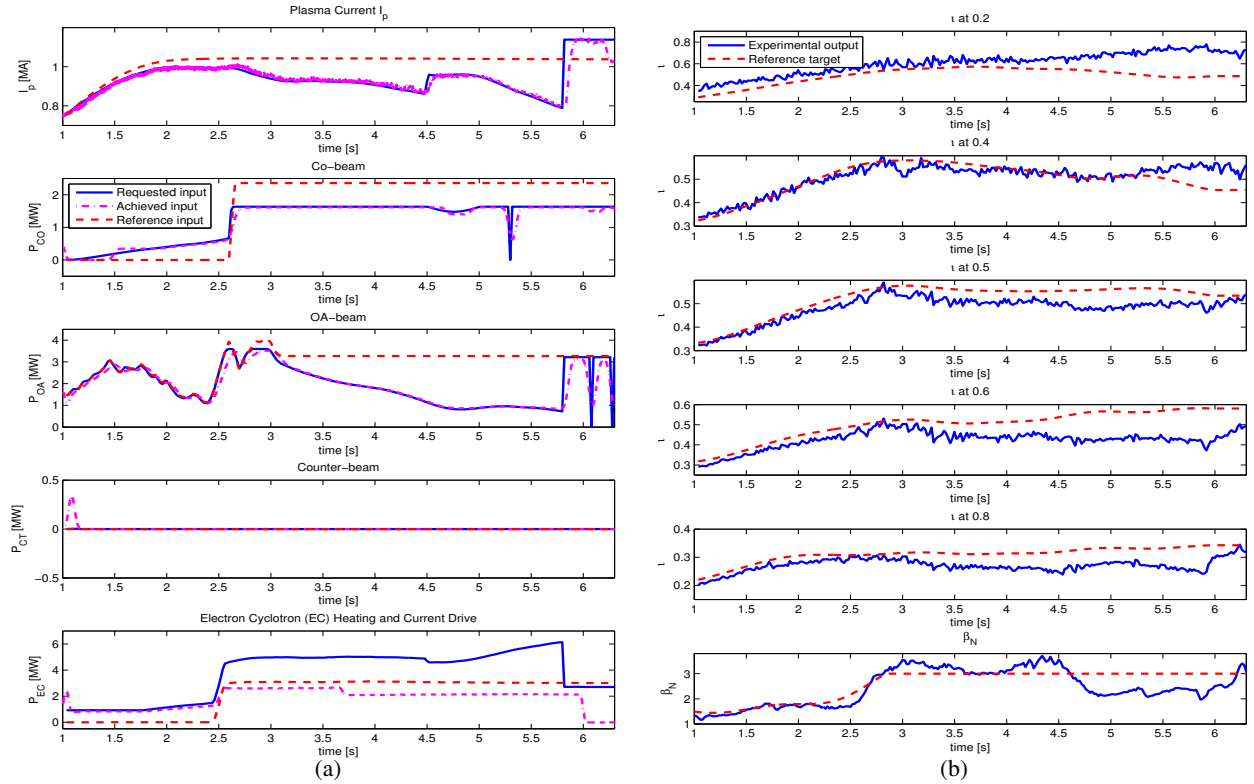

Fig. 5. Rotational transform ι profile and β_N control experiment (shot #150749) with off-axis NBI: (a) Reference (feedforward) inputs (red dashed lines), requested feedforward+feedback control inputs (blue solid lines) and achieved control inputs (magenta dashed-dotted lines); (b) Reference target profile at $\hat{\rho} = 0.2, 0.4, 0.5, 0.6, 0.8$ and β_N (red dashed lines) and experimental closed-loop-controlled ι profile at $\hat{\rho} = 0.2, 0.4, 0.5, 0.6, 0.8$ and β_N (solid blue lines) .

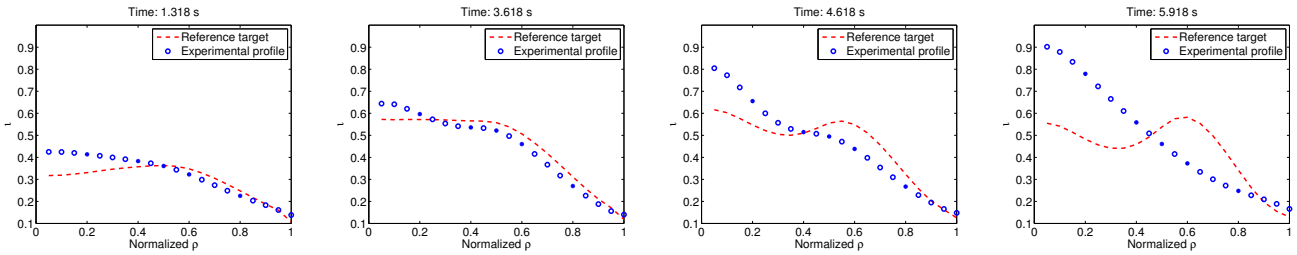

(a) FB ON, Dis. OFF (b) FB ON, Dis. OFF (c) FB ON, Dis. ON (d) FB OFF, Dis. ON

Fig. 6. Plasma $\iota(\hat{\rho})$ profile at time t= 1.318, 3.618, 4.618, 5.918 seconds from shot #150749 on DIII-D.

with these discharge parameters are shown in Fig. 5 (red dashed line). The disturbance was introduced at $t = 4.5$ s, and the feedback controller was active in the interval $[t_i, t_f] = [1, 5.8]$ during the experiment.

Fig. 5 (a) shows the reference (red dashed lines), requested feedforward+feedback inputs (solid blue lines) and achieved inputs (dotted-dashed lines) during the experiment (shot #150749). As shown in Fig. 5 (a.1)-(a.4), the plasma current and the beam powers successfully follow the requested values. During the shot, the total EC power is limited to around 2 MW, but the requested value goes up to 6 MW (Fig. 5 (a.5)). The difference between achieved and requested values of EC power can be interpreted as a large disturbance that the controller must try to overcome. After $t \approx 2.5$ s, the P_{CO} reaches saturation, which activates the anti-windup compensator in an attempt to keep the states of the feedback controller from winding up. The experimental closed-loop-controlled ι profile at $\hat{\rho} = 0.2, 0.4, 0.5, 0.6, 0.8$ and β_N (solid blue lines) are shown in Fig. 5 (b) and compared with the target values (red dashed lines). The controller regulates the ι profile close to the target profile until the disturbance is introduced, even in the current ramp-up phase. The controller drives some of the beams into saturation and requests the plasma current to decrease, which increases the tracking error in the outer part of the ι profile, in order to try to reduce the tracking error in the inner part of the ι profile. When the controller is turned off at $t = 5.8$ s, the actuator values drift away from the feedforward+feedback values immediately. Because the outer ι profile is more quickly influenced by I_p, the tracking errors at $\hat{\rho} = 0.5$, 0.6, and 0.8 become smaller with the increasing of I_p.

The introduction of the off-axis NBI into the experiment placed the plasma in a different operating state with respect to the reference state around which the model was identified. As a result, the validity of the linear plasma model may limit the performance of the model-based controller in this operating scenario. During the closed-loop experiment, the EC power request was not achieved, therefore, the feedback controller output was no longer driving the plant, and as a result, the states of the controller were incorrectly updated. Finally, the actuator saturation during the experiment limited the ability of the feedback controller to manipulate the profile evolution. In order to evaluate the whole ι profile, a series of four plasma profiles at different times during shot #150749 are shown in Fig. 6. Although the model was identified using only data after 2.5 s, the model-based controller performs reasonably well in the current ramp-up phase, which is shown in Fig. 6 (a). Before $t = 4.2$ s, the controller regulates the ι profile close to the target profile (Fig. 6 (b)). After this time, the tracking errors become larger. The input disturbances are injected into the system at $t = 4.5$ s, and the controller decreases the I_p to decrease the ι profile near the plasma boundary in order to attempt to track the desired inner ι profile as shown in Fig. 6 (c). However, the tracking errors increase further as shown in Fig. 6 (d).

VI. Conclusion

A robust, model-based, MIMO, ι profile and β_N controller was designed for DIII-D. The design was based on a linear, identified model for H-mode discharges, including uncertainty. The proposed controller was simulated in PTRANSP, and then the controller was experimentally tested in DIII-D. More experimental tests are needed to assess the appropriateness of using data-driven linear models for current profile control. The sensitivity of the static component of the controller to un-modeled or mis-modeled plasma response and its impact on performance need further analysis.

References

[1] L. Ljung, *System Identification: Theory for the User*. Prentice Hall PTR, 1999.

[2] D. Moreau *et al.*, "A Two Time Scale Dynamic Model Approach for Magnetic and Kinetic Profile Control in Advanced Tokamak Scenarios on JET," *Nuclear Fusion*, vol. 48, no. 106001, 2008.

[3] Y. Yoshida *et al.*, "Momentum Transport and Plasma Rotation Profile in Toroidal Direction in JT-60U L-mode Plasmas," *Nuclear Fusion*, vol. 47, no. 8, pp. 856–863, 2007.

[4] D. Moreau *et al.*, "Plasma Models for Real-time Control of Advanced Tokamak Scenarios," *Nuclear Fusion*, vol. 51, no. 063009, 2011.

[5] W. Shi, W. Wehner, J. Barton, M. Boyer, E. Schuster *et al.*, "Multivariable Robust Control of the Plasma Rotational Transform Profile for Advanced Tokamak Scenarios in DIII-D," in *Proceeding of the 2012 American Control Conference*, 2012.

[6] W. Wehner, C. Xu, E. Schuster *et al.*, "Data-driven Modeling and Feedback Tracking Control of the Toroidal Rotation Profile for Advanced Tokamak Scenarios in DIII-D," in *Proceeding of the 2011 IEEE Multiconference on Systems and Control*, 2011.

[7] W. Shi, W. Wehner, J. Barton, M. Boyer, E. Schuster *et al.*, "A Two-time-scale Model-based Combined Magnetic and Kinetic Control System for Advanced Tokamak Scenarios on DIII-D," in *Proceeding of the 51st IEEE Conference on Decision and Control*, 2012.

[8] R. Hawryluk, "An Empirical Approach to Tokamak Transport," in *Course on Physics of Plasma Close to Thermonuclear Conditions, Varenna, Italy*, 1979.

[9] M. Murakami *et al.*, "Off-axis neutral beam current drive for advanced scenario development in DIII-D," *Nuclear Fusion*, vol. 49, 2009.

[10] A. Packard, "What News with μ: Structured Uncertainty in Multivariable Control," Ph.D. dissertation, UC Berkeley, 1988.

[11] J. Barton, M. Boyer, W. Shi, E. Schuster *et al.*, "Toroidal Current Profile Control During Low Confinement Mode Plasma Discharges in DIII-D via First-Principles-Driven Model-based Robust Control Synthesis," *Nuclear Fusion*, vol. 52, no. 123018, 2012.